Analysis of lift-off height and structure of n-heptane tribrachial flames in laminar jet configuration

Stefano Luca*, Fabrizio Bisetti

Clean Combustion Research Center, King Abdullah University of Science and Technology, Saudi Arabia

Abstract

A set of lifted tribrachial n-heptane flames in a laminar jet configuration are simulated. The simulations are performed using finite rate chemistry and detailed transport, and aim at investigating the propagation of tribrachial flames. Varying the inlet velocity of the fuel, different stabilization heights are obtained, and the dependence of the stabilization height in the inlet velocity is compared with experimental data. A detailed analysis of the flame geometry is performed by comparing the flame structure to that of unstretched premixed flames. Issues related to differential diffusion effects, flame stretch, and transport of heat and mass from the burnt gases to the flame front are discussed.

1 Introduction

A tribrachial flame is an edge flame [1] consisting of two distinct premixed flame wings, one lean and one rich, and a trailing diffusion flame between them. These three branches meet at a point called tribrachial (or triple) point. Flames with a tribrachial structure occur in the presence of mixture fraction gradients ahead of the flame front.

Tribrachial flames play an important role in the stabilization mechanism of laminar [2] and turbulent flames [3] and their propagation is relevant to the partially premixed combustion regime. The propagation and structure of tribrachial flames are affected by the concentration gradient ahead of the flame [4], as the local flame speed varies along the front in response to the changing mixture stoichiometry. Tribrachial flames are curved and the flame front near the tribrachial point is subject to stretch. Theoretical [5, 6], numerical [7, 8], and experimental [4, 8–10] studies have shown that the speed of tribrachial flames decreases with increasing concentration gradients. Depending on the mixture gradient, flame curvature and flow configuration, tribrachial flames may propagate faster or slower than their one-dimensional, unstretched counterparts. Heat release and gas expansion ahead of the flame, heat transfer at the curved front, flame stretch in the presence of non-equal diffusivities, finite rate chemistry, and velocity gradients in the incoming flow are mechanisms known to affect flame propagation. Due to the complex interplay of these mechanisms, which are often difficult to characterize experimentally and numerically, a unified theory on the stabilization and propagation of tribrachial flames has yet to emerge [2].

In this work, we simulate steady, atmospheric, tribrachial flames in the mixing layer downstream of a prevaporized nheptane/nitrogen stream injected into an air coflow. Our computational approach features finite rate chemistry and mixture-average transport (Soret and Dufour effects are neglected). The numerical configuration reproduces the experimental setup and parameters utilized in a recent study on the stabilization of non-autoignited, tribrachial flames in heated laminar jets [11].

Our goal is to analyze the stabilization and structure of tribrachial flames in a real burner geometry, highlighting the interplay of mixture and velocity gradients, flame curvature, stretch, heat transfer at the curved front, and differential diffusion brought by the n-heptane fuel.

The inlet temperature, fuel, and dilution ratio are the same for all cases. Thus, the differences in the flame stabilization are due solely to the varying mixture gradient ahead of the flames as the inlet velocity is varied.

This work extends previous study on the same configuration [12].

2 Configuration

We consider lifted flames stabilized in the mixing layer downstream of an axisymmetric fuel jet in a coflow of air. The details of the geometry and flow parameters are available in Ref. [11].

The burner consists of a central nozzle with inner diameter 3.76 mm and wall thickness 0.5 mm. The fuel jet is surrounded by a coflow of slowly moving air issuing from a honeycomb placed 1 cm below the nozzle exit plane. An enclosure having inner diameter 8.5 cm surrounds the fuel and coflowing air streams. In the experimental setup, the enclosure is a Pyrex cylinder surrounded by thermally-insulating material and extends 50 cm downstream of the nozzle exit plane. In the computations, the streamwise extent of the enclosure is 14 cm and the focus is on flames stabilizing well within the computational domain. The fuel stream consists of prevaporized n-heptane diluted in nitrogen. The n-heptane mole fraction is X_f = 0.035, yielding a stoichiometric mixture fraction Z_{st} = 0.3660. The temperatures of the fuel and air inlet streams are equal and set to T_0 = 700 K for the five flames considered.

* Corrisponding author: stefano.luca@kaust.edu.sa

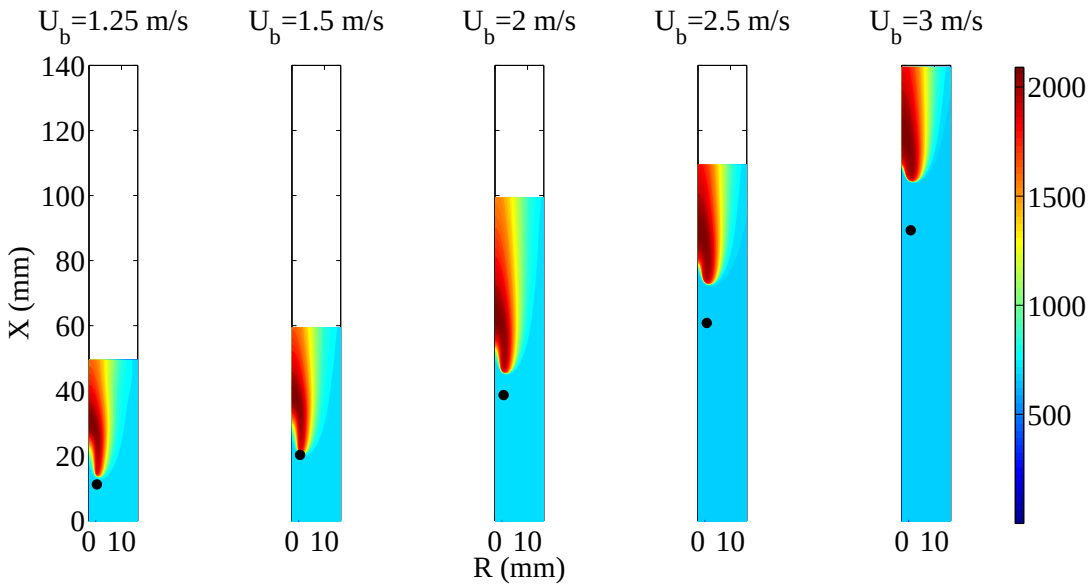

Figure 1: Temperature contours for the five simulations in order of increasing jet bulk velocity (left to right). Black dots: experimental data marking the flame lift-off height corrisponding to the lowest edge of the flame. [11]

The flames differ for the inlet velocity of the fuel stream: the bulk velocity in the nozzle is set equal to $U_b = \{1.25, 1.5, 2, 2.5, 3\}$ m/s and the coflow air velocity U_c is uniform and equal to 0.4 m/s.

3 Methods and models

The gas phase hydrodynamics are modeled with the reactive Navier-Stokes equations in the low Mach number limit [13]. The equations are not shown here for the sake of brevity and may be found in [13]. The transport of heat and mass is described using the Hirschfelder and Curtiss approximation to the diffusive fluxes [13] together with a velocity-correction approach to satisfy mass conservation [14]. The species obey the ideal gas equation of state and the simulations are conducted at atmospheric pressure. All transport properties are computed with a mixture-average approach.

In this work, the mixture fraction Z_B is based on Bilger's definition and reconstructed locally from the mass fraction of all species as in [15]. The elemental mass fraction weights are $\delta_H = 0.5/W_H$, $\delta_C = 2/W_C$, and $\delta_O = 1/W_O$, where $W_{H,C,O}$ are the molecular mass of atomic hydrogen, carbon, and oxygen, respectively.

The parallel finite difference flow solver NGA [16] is used to solve the transport equations. For an in-depth description of the numerical approach and computational details, see Ref. [17]. The equations are discretized in a two-dimensional axisymmetric cylindrical domain using a non-homogeneous, structured mesh. The axial and radial coordinates are x and r, respectively. In the region where the tribrachial flame stabilizes, the mesh is homogeneous in the axial and radial directions with grid size $\Delta x = \Delta r = 10$ μm. Outside of this region, the computational mesh is stretched. The total number of points is $N_x \times N_r = \{1.04, 1.07, 1.21, 1.57, 1.69\} \times 10^6$ for the five cases considered.

The convective and diffusive terms in the momentum equation are discretized with a second order finite differences centered scheme. The convective term in the scalar equations is discretized with a WENO5 [18] scheme and the diffusive fluxes are treated with a second order centered scheme. As the solution is marched to steady state, the time step size is constant and equal to 0.5 μs, guaranteeing a CFL number for the convective terms well below unity (O(0.1)) and moderately large Fourier numbers for the viscous and diffusive fluxes (O(10)).

In the computational domain, inflow conditions are applied at a plane located 1 cm below the nozzle exit, consistently with the geometry of the experimental setup. The boundary conditions are imposed inflow at x = 0 (Poiseuille flow in the nozzle and uniform flow in the coflow) and free convective outflow at the top boundary. No-slip, adiabatic, and impermeable wall conditions are imposed on the inner and outer fuel nozzle walls and along the surface of the surrounding enclosure.

The solver relies on an MPI-based distributed memory parallelization strategy and is executed in parallel on the Linux clusters "Noor" and "Smc" available at the Clean Combustion Research Center. In order to reach steady state, the most demanding case requires approximately 360 hrs in wall-clock time (or 45,000 cpu-hours) on 128 processing cores of Intel Xeon X5570 quad-core processors.

4 Results

Fig. 1 shows contours of temperature for the set of flames simulated. For each simulation is shown the temperature in the entire domain that varies to adapt to the flame height. Increasing the inlet velocity of the fuel stream the flame stabilize further downstream. With

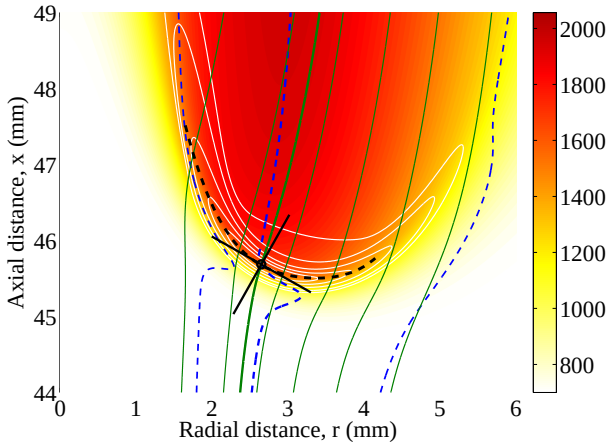

Figure 2: Temperature contour for the flame with $U_b = 2$ m/s. Solid: white: heat release rate isocontour; Green: streamlines; black: tangent and normal to the flame front in the triple point; Dashed: blue: Z_B isoline; black: flame front

black dots are reported experimental data from [11].

Fig. 2 shows an overview of the flame with inlet bulk velocity $U_b = 2$ m/s. It is shown the contour of the temperature, the isoline of heat release rate (from the peaks of heat release rate is defined the flame front), the Bilger mixture fraction isoline (lean and rich flammability limits and stoichiometry), and the flow streamlines. Stoichiometric isoline and flame front meet at the tribrachial point: where are reported normal and tangent to the flame front. The flame is tilted with respect to the axial direction, and stabilize downstream (about 45.5 mm above the nozzle in this case); the heat release rate isolines show the two premixed wings while the diffusion flame is not visible due to the dilution of the fuel stream.

Fig. 3 shows the comparison between two of the flames. Those are the flames with the smallest and greatest velocity in the set of flames simulated. As shown, both flames present a rich and a lean premixed flames but the diffusion flames are not visible, due to the highly diluited fuel stream.

As the velocity U_b decreases the flame stabilizes closer to the nozzle (about 14 mm compared to 104 mm) and experiences a higher velocity gradient and mixture fraction gradient ahead of the flame front. The velocity gradient ahead of the flame is responsible for the tilt of the flame with respect to the axial direction: flames that stabilize closer to the nozzle will experience higher velocity gradients and more tilt; similarly the mixture fraction gradient results in a curved front with smaller radius of curvature for flame, which are closer to the nozzle.

Fig. 3 shows that the maximum value of the heat release rate is smaller for the flame that stabilizes closer to the nozzle meaning that the flame is weaker than flames that stabilize further downstream. It is worth noting that the two flames differ only for the inlet velocity of the fuel stream, everything else being equal.

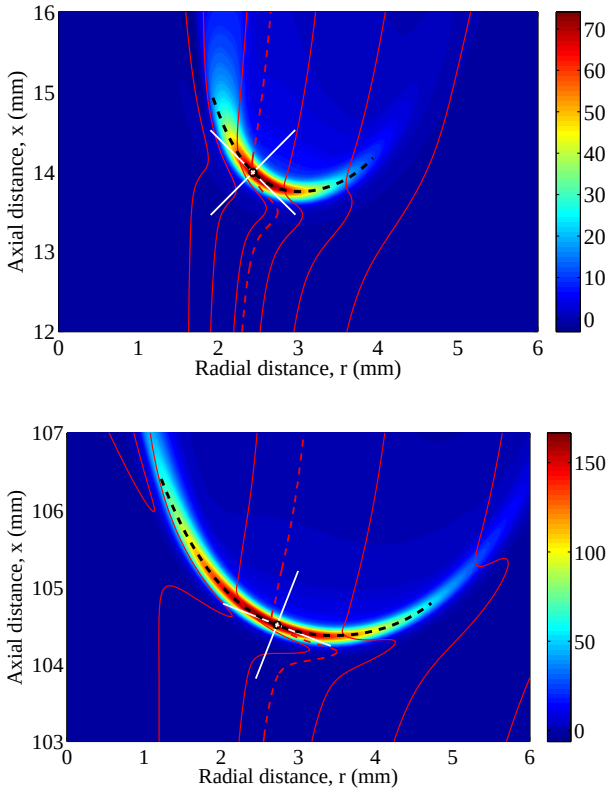

Figure 3: Top: $U_b = 1.25$ m/s. Bottom: $U_b = 3$ m/s. Heat release rate contour. Red solid: Z_B isoline, red dashed: $Z_B = Z_{st}$, black dashed: flame front, white solid: normal and tangent to the flame front in the triple point

Based on the definition of the flame front as the location of peak heat release rate, we may compute quantities along the normal to the flame front through the tribrachial point and along the front itself.

Fig. 4 shows the flow velocity and the Bilger's mixture fraction along the normal to the flame front through the tribrachial point.

Flow slows down approaching the flame due to the expansion related to heat release: since the maximum heat release rate is higher for flames far from the nozzle, as shown, the velocity increase is greater for flames that stabilize further downstream.

Regarding Z_B, the mixture fraction increases ahead of the flame and then decreases; this behaviour is more pronounced for the flame closest to the nozzle and it is due to the fact that the flames are tilted.

Due to flame tilt, the normal extends into the fuel stream, thereby resulting in an increase of Z_B along the normal. For this reason, the analysis of the flame structure along the normal to the flame front is informative for flames having moderate to no tilt, but somewhat misleading for the flames with significant tilt. Thus, flame analysis is performed along the flame front as well.

Fig. 5 shows heat release rate and the normal component of the burning velocity along the flame front

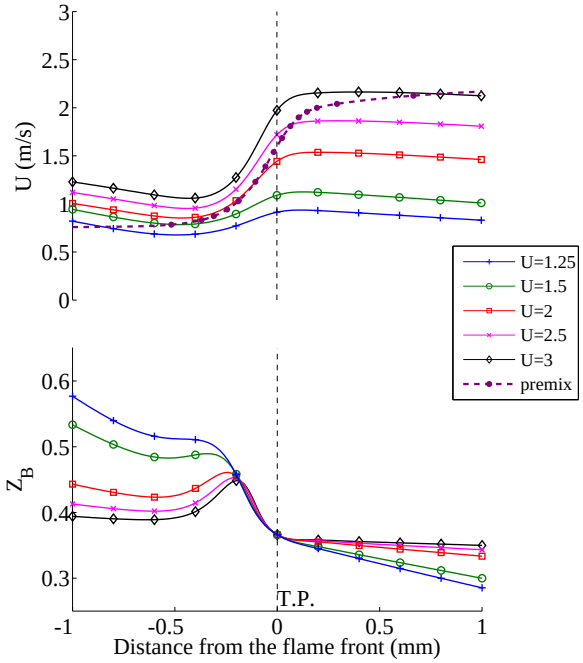

Figure 4: Quantities along the normal to the flame front for all five flames and solution of a freely propagating 1D premixed flame. Top: Velocity; Bottom: Bilger's mixture fraction

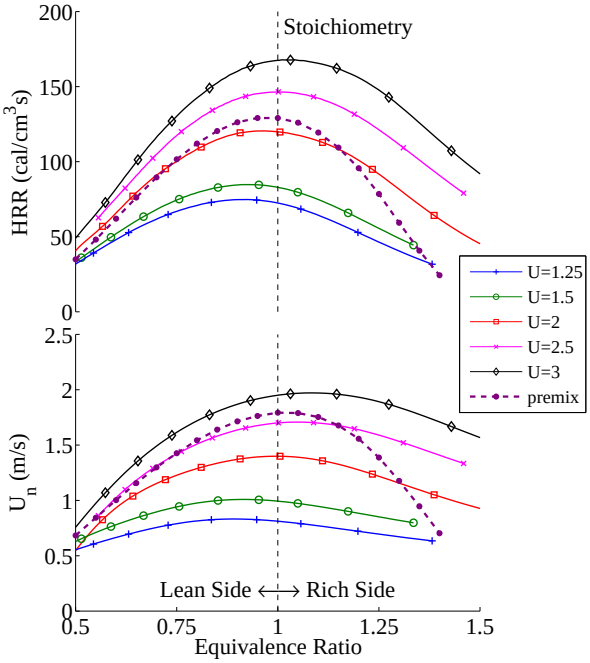

Figure 5: Quantities along the flame front of the five flames and solution of a freely propagating 1D premixed flame. Top: Normal burning velocity; Bottom: Heat release rate

parametrized with the equivalence ratio. The burning velocity is defined as the flow velocity at the location of peak heat release rate [19]. As shown in Fig. 5 for all cases, the dependence of the heat release rate on the local mixture stoichiometry along the flame front is similar to that found in freely propagating premixed flame on the lean side. On the rich side, instead, the flames differ from the premixed one and the difference is greater the farther the flame is from the nozzle.

The same trends are apparent for the normal burning velocity, also shown in Fig. 5. Furthermore, for flames that stabilize further from the nozzle the difference between lean side and rich side is greater.

From those results we conclude that heat release rate and burning velocity are enhanced on the rich side and this enhancement is greater for flames that stabilize further downstream.

Along the flame front it is also possible to define and compute [20] the stretch as:

$$\kappa = -\mathbf{nn} : \nabla\mathbf{u} + \nabla \cdot \mathbf{u} + \mathbf{u_n}\nabla \cdot \mathbf{n} \qquad (1)$$

Normalizing the stretch by the local time scale in the unstretched 1D flame, the local Karlovitz number is obtained:

$$\mathrm{Ka} = \kappa \frac{\delta_0}{s_0} \qquad (2)$$

In Fig. 6 the local Karlovitz number is shown along the flame front, parametrized with the equivalence ratio.

On the lean side all five simulations display a Karlovitz number almost constant and close to one. On the rich side, instead, the Karlovitz number shows the same trend for the five flames: Ka increases moving towards richer mixtures on the rich wing of the tribrachial flame.

According to the theory on the effects of flame stretch on flame propagation for large hydrocarbon species in air [21], positive stretch enhances the burning velocity on the rich premixed wing. Furthermore, based on the Karlovitz number on the rich side, the flame enhancement is greater for flames stabilized further downstream.

5 Conclusions

A set of five lifted tribrachial n-heptane flames stabilized in the mixing layer of a round laminar jet of diluted n-heptane is simulated with finite rate chemistry and detailed transport. The flames differ for the inlet velocity of the fuel stream.

The numerical configuration and parameters reproduce an experimental setup for which published data are available [11].

As the inlet velocity decreases the flame stabilizes closer to the nozzle and larger velocity and mixture fraction gradients ahead of the flame are established. Due to the velocity gradient, the tilt of the flame increases closer to the nozzle, while the radius of curvature given by the mixture fraction gradient decreases.

An analysis of selected quantities along the normal to the flame front in the tribrachial point and along the

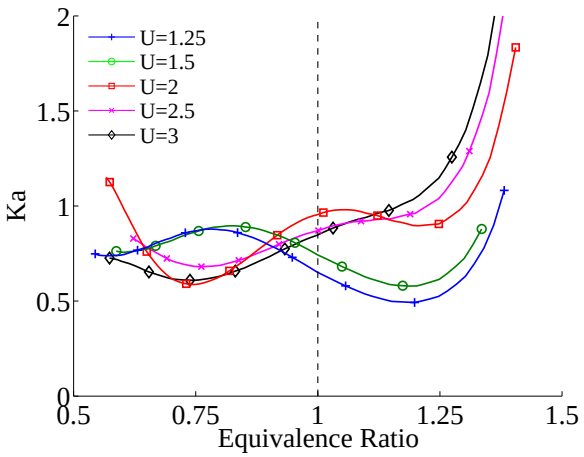

Figure 6: Local Karlovitz number along the flame front for all five flames

flame front is performed: flames that stabilize further downstream present greater heat release rate resulting enhanced, in particular on the rich side.

Furthermore, flames far from the nozzle present higher burning velocity, while the flame with the smallest inlet velocity, that presents the smallest radius of curvature and stabilizes closest to the nozzle, is weakened.

Considerations on the Karlovitz number confirm highly stretched flames on the rich side that explain the enhancement of the burning velocity for flames that stabilize further downstream.

Acknowledgments

The research reported in this paper was supported by King Abdullah University of Science and Technology (KAUST).

References

[1] J. Buckmaster, Prog. Energ. Combust. Sci. 28 (2002) 435–475.

[2] S. H. Chung, Proc. Combust. Inst. 31 (2007) 877–892.

[3] K. M. Lyons, Prog. Energ. Combust. Sci. 33 (2007) 211–231.

[4] Y. Ko, S. Chung, Combust. Flame 118 (1999) 151–163.

[5] J. Dold, Combust. Flame 76 (1989) 71–88.

[6] L. J. Hartley, J. Dold, Combust. Sci. Technol. 80 (1991) 23–46.

[7] G. R. Reutsch, L. Vervisch, A. Linan, Phys. Fluids 7 (1995) 1447–1454.

[8] X. Qin, C. W. Choi, A. Mukhopadhyay, I. K. Puri, S. K. Aggarwal, V. R. Katta, Combust. Theor. Model. 8 (2004) 293–314.

[9] M. K. Kim, S. H. Won, S. H. Chung, Proc. Combust. Inst. 31 (2007) 901–908.

[10] I. A. Mulla, S. R. Chakravarthy, Combust. Flame 160 (2013) 1345–1356.

[11] S. K. Choi, S. H. Chung, Combust. Flame 160 (2013) 1717–1724.

[12] F. Bisetti, S. M. Sarathy, M. Toma, S. H. Chung, Proc. Combust. Inst. 35 (2015) 1023–1032.

[13] T. Poinsot, D. Veynante, Theoretical and Numerical Combustion, R.T. Edwards, Philadelphia, 2 edition (2005).

[14] T. P. Coffee, J. M. Heimerl, Combust. Flame 43 (1981) 273–289.

[15] F. Bisetti, J.-Y. Chen, J. H. Chen, E. R. Hawkes, Proc. Combust. Inst. 32 (2009) 1465–1472.

[16] O. Desjardins, B. Blanquart, G. Balarac, H. Pitsch, J. Comput. Phys. 227 (2008) 7125–7159.

[17] A. Attili, F. Bisetti, M. Mueller, H. Pitsch, Combust. Flame 161 (2014) 1849–1865.

[18] G.-S. Jiang, C.-W. Shu, J. Comput. Phys. 126 (1996) 202–228.

[19] J. Tien, M. Matalon, Combust. Flame 84 (1991) 238–248.

[20] S. M. Candel, T. J. Poinsot, Combust. Sci. Technol. 70 (1990) 1–15.

[21] C. Law, C. Sung, Prog. Energ. Combust. Sci. 26 (2000) 459–505.